Acta Crystallographica Section D
Biological Crystallography
ISSN 0907-4449

A hydrogen-bonding network is important for oxidation and isomerization in the reaction catalyzed by cholesterol oxidase

Artem Y. Lyubimov,[a]‡ Lin Chen,[b] Nicole S. Sampson[b] and Alice Vrielink[c]*

[a]Department of Molecular, Cell and Developmental Biology, University of California, Santa Cruz, Sinsheimer Laboratories, 1156 High Street, Santa Cruz, CA 95064, USA, [b]Department of Chemistry, Stony Brook University, Stony Brook, NY 11794-3400, USA, and [c]School of Biomedical, Biomolecular and Chemical Sciences, University of Western Australia, 35 Stirling Highway, Crawley, WA 6009, Australia

‡ Present address: Department of Molecular and Cell Biology, University of California, Berkeley, 360 Stanley Hall, Berkeley, CA 94720, USA.

Correspondence e-mail: alice.vrielink@uwa.edu.au

Received 30 July 2009
Accepted 16 September 2009

PDB References: cholesterol oxidase, N485D mutant, 3gyi, r3gyisf; N485L mutant, 3gyj, r3gyjsf.

Cholesterol oxidase is a flavoenzyme that catalyzes the oxidation and isomerization of 3β-hydroxysteroids. Structural and mutagenesis studies have shown that Asn485 plays a key role in substrate oxidation. The side chain makes an NH$\cdots\pi$ interaction with the reduced form of the flavin cofactor. A N485D mutant was constructed to further test the role of the amide group in catalysis. The mutation resulted in a 1800-fold drop in the overall k_{cat}. Atomic resolution structures were determined for both the N485L and N485D mutants. The structure of the N485D mutant enzyme (at 1.0 Å resolution) reveals significant perturbations in the active site. As predicted, Asp485 is oriented away from the flavin moiety, such that any stabilizing interaction with the reduced flavin is abolished. Met122 and Glu361 form unusual hydrogen bonds to the functional group of Asp485 and are displaced from the positions they occupy in the wild-type active site. The overall effect is to disrupt the stabilization of the reduced FAD cofactor during catalysis. Furthermore, a narrow transient channel that is shown to form when the wild-type Asn485 forms the NH$\cdots\pi$ interaction with FAD and that has been proposed to function as an access route of molecular oxygen, is not observed in either of the mutant structures, suggesting that the dynamics of the active site are altered.

1. Introduction

Bacterial cholesterol oxidase is a bifunctional flavoenzyme which catalyzes the oxidation and 1,3-allylic isomerization of 3β-hydroxysterols (Fig. 1). The enzyme serves a primary metabolic function in actinomycetes such as *Brevibacterium* and *Streptomyces* that use cholesterol as a carbon source. In pathogenic bacteria such as *Rhodococcus equi*, an opportunistic pathogen that infects AIDS patients (Linder, 1997), cholesterol oxidase may be utilized as a means of escape from macrophages (Navas *et al.*, 2001). As it is unique to bacteria, cholesterol oxidase is an attractive target for novel antibiotics. A detailed understanding of the active site and its interactions with the substrate and the flavin cofactor during catalysis is necessary for the design of efficient inhibitors.

The cholesterol oxidases from *R. equi* (previously misidentified as *Brevibacterium sterolicum*; Navas *et al.*, 2001) and *Streptomyces* sp. are monomeric proteins (55 kDa) that contain one noncovalently bound FAD molecule per active site (Tomioka *et al.*, 1976; Uwajima *et al.*, 1974). The primary sequences of these enzymes are ~60% identical and their structures exhibit no significant differences (Vrielink *et al.*, 1991; Yue *et al.*, 1999). The catalytic mechanism, which has recently been subject to some re-interpretation (Lario *et al.*,

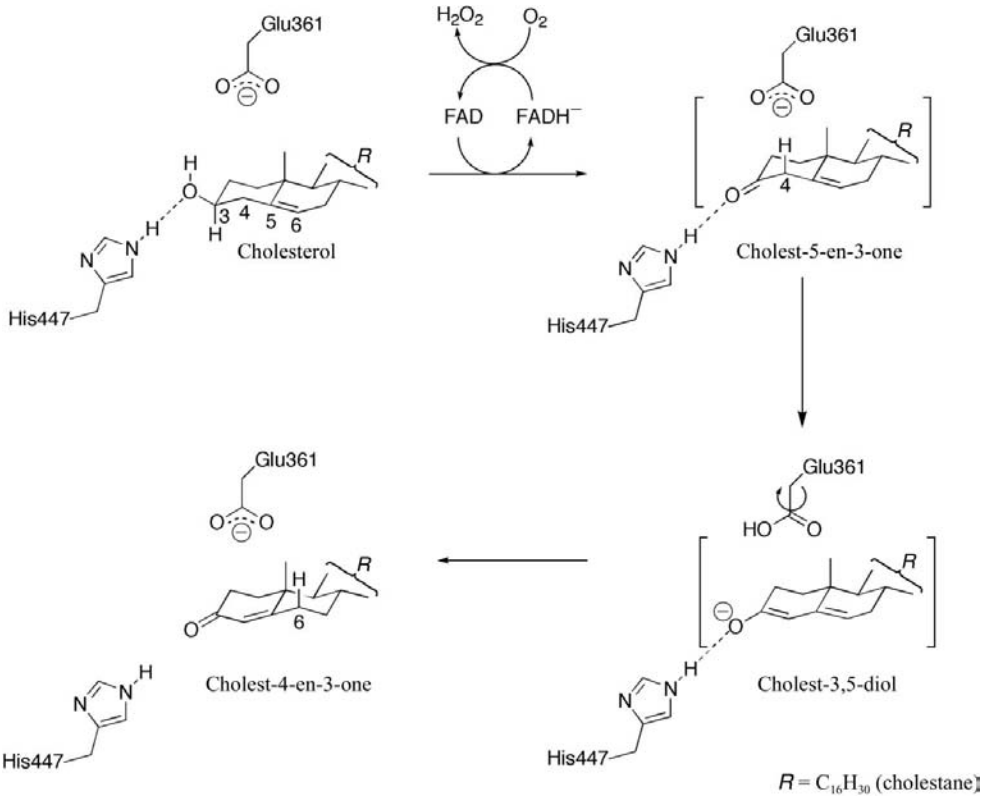

Figure 1
Catalytic mechanism of cholesterol oxidase.

2003), is shown in Fig. 1. Previously, it has been shown by a combination of mutagenesis, kinetics and structural studies that Asn485 is important for efficient substrate oxidation. Mutation of Asn485 to leucine caused a 1100-fold decrease in the k_{cat} of the enzyme, as well as a reduction of the redox potential by 85 mV. A 1.5 Å resolution crystal structure of the N485L mutant suggested that Asn485 stabilizes the reduced FAD *via* an NH$\cdots\pi$ interaction and thus plays a role in the modulation of the flavin's redox potential (Yin *et al.*, 2001).

A subsequent atomic resolution (0.95 Å) crystal structure of the wild-type (WT) enzyme revealed that in order to interact with the reduced FAD the functional group of Asn485 moves closer to the pyrimidine ring of the isoalloxazine moiety (Lario *et al.*, 2003). The reorientation of the asparagine side chain results in movements of a series of other side chains, opening a narrow channel leading from bulk solvent to the isoalloxazine moiety. In the 0.95 Å WT enzyme structure the side chains involved in forming the channel and gating access to the channel exhibit two distinct conformations (designated *A* and *B*). In conformation *A* the side chain of Asn485 is positioned away from the pyrimidine moiety of the FAD cofactor. This repositions a series of side chains extending away from the active site to the surface of the protein such that the channel is closed and there is no access to the active site from the external surface of the molecule. In conformation *B*, the movement of the side chain of Asn485 closer to the pyrimidine ring and the resulting stabilization of the reduced form of the cofactor is accompanied by movements of a series of other residues, including a reorientation of Phe359. These movements result in an opening of the channel, thus providing a potential access route from the external surface of the protein to the buried active site containing the FAD cofactor. This gated channel has been proposed to act as an access route for molecular oxygen. Oxygen is required to oxidize the reduced cofactor during the oxidative half-reaction and controlled access to the active site is important as the cholest-5-en-3-one intermediate is susceptible to radical chain oxidation. These observations suggest that Asn485 plays a significant role in both the reductive and the oxidative half-reactions catalyzed by the enzyme.

To further investigate the role of electrostatics in the active site during the oxidative and reductive half-reactions, Asn485 was mutated to aspartate and the mutant was analyzed by a combination of kinetics, potentiometry and atomic resolution crystallography. To enable a rigorous comparison, the kinetic and potentiometric characterization of the N485L mutant was repeated and its structural interpretation was extended to atomic resolution. The results show that in addition to the disruption of the electrostatic environment around the FAD cofactor, mutations of Asn485 cause substantial changes to the proton-relay network in the active site that impact the formation of the oxygen-access channel.

2. Materials and methods

2.1. Materials

Bovine albumin (BSA) was from Sigma (St Louis, Missouri, USA). Triton X-100 was purchased from Aldrich Fine Chemical Co. (Milwaukee, Wisconsin, USA). Cholesterol was purchased from Sigma Chemical Co. (St Louis, Missouri, USA). Restriction endonucleases, T4 DNA ligase and calf intestinal alkaline phosphatase were purchased from New England Biolabs (Beverly, Massachusetts, USA). Oligonucleotides were purchased from IDT Inc. (Coralville, Iowa, USA). Dyes for redox-titration experiments were purchased from Sigma (St Louis, Missouri, USA). All other chemicals and solvents, of reagent or HPLC grade, were supplied by Fisher Scientific (Pittsburgh, Pennsylvania, USA). Water for assays and chromatography was distilled, followed by passage through a Barnstead NANOpure filtration system.

2.2. Buffers and media

10× PBS: 137 m*M* NaCl, 4.3 m*M* Na_2HPO_4, 2.5 m*M* KCl, 1.4 m*M* KH_2PO_4 in deionized distilled H_2O. 10× HEPES: 1.37 *M* NaCl, 0.06 *M* D(+)-glucose, 0.05 *M* KCl, 0.007 *M* $Na_2HPO_4{\cdot}7H_2O$, 0.2 *M* HEPES pH 7.1. LB medium: 10 g tryptone, 5 g yeast extract, 5 g NaCl, 1 ml 1 *N* NaOH in 1 l deionized distilled H_2O. Buffer *A*: 50 m*M* sodium phosphate pH 7.0. Buffer *B*: 50 m*M* sodium phosphate, 2 *M* ammonium sulfate pH 7.0. Buffer *C*: 100 m*M* citrate–phosphate pH 5.1; the ionic strength was adjusted to the same level as buffer *A* with 5 *M* NaCl to a final conductivity of 10 mS cm^{-1}.

2.3. General methods

Restriction digests and ligations were performed according to the procedures described below. The plasmids were purified with the Wizard Plus DNA Purification System (Promega, Madison, Wisconsin, USA). A Shimadzu UV2101 PC Spectrophotometer was used for assays and acquisition of UV spectra. Fluorescence measurements were taken on a Spex Fluorolog 3-21 spectrofluorometer.

2.4. Construction of the N485D mutant expression plasmid pCO300

A 214-base oligonucleotide was made by PCR using two primers. Primer 1 contained the designated mutation site and an *Stu*I site (5′-ggCTggggCCCCAACggTAACATCATgACCgCCCgggCCAACCACATgTggAACCCCACCggCgCCC-3′). Primer 2 corresponded to the anticoding strand and contained a *Hin*dIII site (5′-gCTCACAAgCTTACgACgCCgTgACgTCCTgCTTgATgATgCgCTCgACgTTCCgCTCggCCAgCgCCgTgATggTCACgAACgggAggACgCCgACgg-3′). Using these two primers with *Xho*I-restricted pCO202 (Kass & Sampson, 1998) as a template, 35 cycles of PCR were performed with iProof polymerase (Bio-Rad Laboratories, Hercules, California, USA) at an annealing temperature of 345 K. The PCR fragment was digested with *Stu*I and *Hin*dIII, purified and subcloned into pCO200 (Kass & Sampson, 1998) that had been similarly digested to yield the N485D ChoA mutant expression plasmid pCO300. Sequencing of the clone was conducted at the Stony Brook sequencing facility using an ABI 3730 Genetic Analyzer (Applied Biosystems, Foster City, California, USA).

2.5. Protein purification of WT and mutant cholesterol oxidases

Escherichia coli BL21(DE3)plysS cell paste was obtained from 1 l 2×YT–ampicillin (200 µg ml^{-1} ampicillin) medium grown at 301 K for 10 h after addition of IPTG (100 µg ml^{-1}) at A_{600} = 0.6 by centrifugation at 4000*g* for 30 min. The pellet was resuspended in buffer *A* and lysed using a French press at 124 MPa. All subsequent steps were conducted at 277 K. Cell debris was removed by centrifugation at 135 000*g* for 60 min. The supernatant was precipitated with 1.0 *M* ammonium sulfate and the pellet was discarded. Ammonium sulfate was added to the supernatant to a final concentration of 2 *M*. The pellet was obtained by centrifugation at 4000*g*. This pellet was resuspended in buffer *A* (5 ml) and desalted using dialysis (nominal molecular-weight cutoff 6000–8000) against buffer *A*. The dialysate was loaded onto a column of DEAE-cellulose (30 × 25 cm; DE-52, Whatman) pre-equilibrated with buffer *A*. Fractions were collected by elution with buffer *A* (100 ml). Fractions containing cholesterol oxidase (as determined by SDS–PAGE) were combined and concentrated by ammonium sulfate precipitation (3.0 *M*). The pellet was redissolved in buffer *A* to give a final concentration of between 10 and 20 mg ml^{-1} protein and was further purified on a butyl-Sepharose column (30 ml butyl-Sepharose-4 Fast Flow, XK 16/40, Pharmacia Biotech, Uppsala, Sweden) pre-equilibrated with buffer *B*. The protein was eluted by running a linear gradient from 75% buffer *B* to 100% buffer *A* (160 ml). Fractions (4 ml) were collected and the elution profile was monitored at A_{280}. The fractions were assayed for content and purity by SDS–PAGE. Fractions containing pure cholesterol oxidase (>98%) were combined and ultrafiltered (YM30 membrane) into buffer *A*.

2.6. Crystallization, data collection and processing

Crystals of both mutants were obtained by the vapor-diffusion method using identical conditions as used for the WT enzyme (Yue *et al.*, 1999): 9–11% polyethylene glycol (PEG) 8000, 75 m*M* $MnSO_4$ and 100 m*M* sodium cacodylate pH 5.2. Crystals suitable for data collection grew within approximately two weeks. Surprisingly, crystals of the N485D mutant degraded within approximately a month of formation, so data were collected as soon as crystals of suitable size were obtained.

Data were collected on Stanford Synchrotron Radiation Laboratory (SSRL) beamlines 9-2 (N485L) and 11-1 (N485D). In each case, a complete data set was collected from a single crystal. Prior to data collection, crystals were immersed for ∼5 s in a cryoprotectant solution composed of the original precipitant solution with the addition of 20% glycerol in the case of the N485L mutant and 20% PEG 400 in the case of the N485D mutant. The crystals were then flash-frozen in liquid N_2 and mounted on the goniostat in preparation for data collection.

In each case, data were collected in two sweeps: one at low exposure to avoid overloaded reflections at low resolution and one at high exposure to attain the highest possible resolution. In each case, a complete atomic resolution data set was obtained. X-ray diffraction images were processed with the *HKL*-2000 suite of software (Otwinowski & Minor, 1997); the final crystallographic data statistics are summarized in Table 1.

2.7. Structure solution and refinement

The same solution and refinement procedure was followed for both structures. Difference Fourier techniques were used to solve the structure using a starting model adapted from the 0.95 Å resolution structure of the WT enzyme (PDB code 1mxt; Lario *et al.*, 2003). This model was modified as follows: all anisotropic *B*-factor parameters were removed and the side

Table 1
Crystallographic data and refinement statistics.

	N485L	N485D
Data collection		
Space group	$P2_1$	$P2_1$
Unit-cell parameters (Å, °)	a = 51.29, b = 73.40, c = 63.14, α = 90.0, β = 105.15, γ = 90.0	a = 51.28, b = 72.78, c = 62.97, α = 90.0, β = 105.12, γ = 90.0
Resolution (Å)	36.69–0.92 (0.94–0.92)	30.40–1.00 (1.02–1.00)
No. of reflections (total)	801838	1093327
No. of reflections (unique)	291838	231276
R_{merge}	0.048 (0.370)	0.069 (0.543)
$I/\sigma(I)$	25.5 (3.03)	21.7 (1.5)
Completeness (%)	92.7 (88.0)	96.2 (58.9)
Redundancy	2.8 (2.1)	4.7 (2.5)
Refinement		
R_{work}/R_{free}	12.3/15.1	12.6/15.8
No. of atoms		
Protein	9063	8775
Ligand/ion	90	82
Water	604	682
Data-to-parameter ratio	5.61	4.48
Isotropic B factors (Å^2)		
Protein (main chain)	9.49	13.58
Protein (side chain)	12.85	18.62
FAD	5.9	11.2
R.m.s. deviations		
Bond lengths (Å)	0.014	0.014
Bond angles (Å)	0.030	0.030
Planarity (Å^3)	0.095	0.090
Alternative conformations	113	108

chains of Asn485, Met122, Val124, Val191, Phe359, Leu377, His447 and Asp459 were changed to alanines. Finally, the FAD cofactor and all solvent molecules (including water, glycerol and sulfate) were removed.

The starting model was subjected to a round of rigid-body refinement in *REFMAC*5 (Murshudov *et al.*, 1997). At this point, the FAD cofactor, most of the truncated side chains and many structural water molecules could be seen as prominent difference electron-density features. These moieties were modeled where best represented by the electron density and the resulting structure was refined using isotropic B factors in *REFMAC*5. Manual modeling, as well as local real-space refinement, was carried out using the program *Coot* (Emsley & Cowtan, 2004).

As the phases improved during the course of refinement, many alternate conformations of amino-acid residues became evident in the electron-density maps. Further refinement was carried out using the program *SHELX* (Sheldrick, 2008). The free R values were monitored during the course of refinement of each structure. For each structure, a test data set was created from 5% of reflections selected randomly from the total set of collected data. A significant improvement in R values and electron-density map quality was observed when anisotropic temperature factors were refined for all non-H atoms in the structure. In the case of water molecules, anisotropic temperature-factor parameters were restrained by using the ISOR and CONN commands.

Water molecules were added where strong peaks of electron density were observed and where at least one reasonable hydrogen bond was formed to the protein, FAD cofactor or other water molecules. Alternate positions for some water molecules were modeled where indicated by persistent electron density. If alternate positions of water molecules corresponded to alternate positions of amino-acid residues, the same free variable (FVAR) was used to refine the occupancy for the water molecule and the amino-acid conformers.

Alternate conformations were added where clearly indicated by electron-density peaks. Model bias was minimized by initially refining multiple side-chain conformations using isotropic temperature factors; subsequent rounds of refinement included the anisotropic parameters for these residues. Alternate conformations of different residues that were likely to coexist were assigned the same part number (*e.g. A* or *B*) in such a way as to avoid steric clashes and (when applicable) to maximize favorable interactions between these residues. Partial occupancy was determined in *SHELXL* by assigning a free occupancy variable (FVAR) to each residue exhibiting alternate conformations and refining it such that the sum of partial occupancies amounted to unity.

The data-to-parameter ratio attainable at this resolution does not allow the positional refinement of H atoms, which were modeled in 'riding positions', where the hydrogen coordinates are constrained with respect to the atom the hydrogen is bonded to. H atoms were introduced in three steps after the anisotropic model including all non-H atoms was refined to convergence. Firstly, all H atoms bonded to main-chain N and CA atoms as well as to all side-chain C atoms were introduced. Next, H atoms bonded to N and O atoms of Asn, Gln, Ser, Thr, Trp and Tyr were modeled. Finally, FAD H atoms were introduced, along with titratable H atoms of histidine side chains, which were modeled only where electron density was visible at a contour above 2.0σ. Introduction of H atoms improved the R values by ∼1.5% and resulted in the detection of a few additional weak alternate conformations for some amino-acid residues.

The high flux of intense X-rays used during data collection from the N485L crystals resulted in strong radiation damage throughout the molecule. Persistent negative difference density could be seen on many solvent-exposed glutamate, aspartate, threonine and serine functional groups. To account for decarboxylation and dehydroxylation of these residues, the functional groups were modeled at 50 or 75% occupancy.

The final models were validated using the programs *SFCHECK* (Vaguine *et al.*, 1999) and *PROCHECK* (Laskowski *et al.*, 1993) from the *CCP*4 suite of software (Collaborative Computational Project, Number 4, 1994). The final refinement statistics are given in Table 1. The solvent-accessible surface shown in Fig. 4 was calculated using the program *SPOCK* (Christopher, 1998) and rendered using *MolScript* (Kraulis, 1991) and *Raster3D* (Merritt & Bacon, 1997). *PyMOL* (DeLano, 2002) was used to render molecular models and electron-density maps. The structures have been deposited in the Protein Data Bank (Berman *et al.*, 2000) with the accession codes 3gyj for the N485L mutant and 3gyi for the N485D mutant.

Table 2
Michaelis–Menten rate constants for WT and mutant cholesterol oxidases.

		Oxidation†				Isomerization‡			
	Enzyme	k_{cat} (s^{-1})	K_m^{app} (μM)	k_{wt}/k_{mutant}	k_{cat}/K_m^{app} pH 5.1/pH 7.0	k_{cat} (s^{-1})	K_m^{app} (μM)	k_{wt}/k_{mutant}	k_{cat}/K_m^{app} pH 5.1/pH 7.0
pH 7.0	WT	47 ± 4.0	2.7 ± 0.28	n.a.		61 ± 3.9	7.2 ± 1.4	n.a.	
	N485D	0.073 ± 0.0048	6.6 ± 1.2	644		10 ± 0.47	7.2 ± 0.87	6.1	
	N485L	0.044 ± 0.0051	4.6 ± 1.9	1068		3.2 ± 0.3	18 ± 0.6	19	
pH 5.1	WT	46 ± 3.6	6.7 ± 1.4	n.a.	0.44	64 ± 3§	6.2 ± 0.7§	n.a.	1.2
	N485D	1.4 ± 0.16	6.3 ± 2.1	33	20	1.1 ± 0.086	5.9 ± 1.3	58	0.134
	N485L	0.035 ± 0.0044	6.2 ± 2.2	1314	0.59	2.5 ± 0.16	8.5 ± 1.1	26	0.78

† Measured by H_2O_2 formation with cholesterol as substrate. ‡ Measured by cholest-4-en-3-one formation at 240 nm with cholesten-5-en-3-one as substrate. § Kass and coworkers (Kass & Sampson, 1998).

2.8. UV and fluorescence measurements of WT and mutant cholesterol oxidases

Solutions of cholesterol oxidase were prepared in buffer *A*. For steady-state enzyme kinetics, the initial velocities of the WT and mutant cholesterol oxidases were measured in one of two ways at 310 K. (i) The formation of conjugated enone was followed as a function of time at 240 nm (ε_{240} = 12 100 M^{-1} cm^{-1}). Triton X-100 was added to buffer *A* to a final concentration of 0.025%(*w*/*v*) with 0.01%(*w*/*v*) BSA. The detergent micelles were allowed to form at 310 K for 10 min, cholesterol or cholest-5-en-3-one was added from a 2-propanol stock solution and the assay mixture was equilibrated for 10 min. The reaction was initiated by adding cholesterol oxidase (WT or mutant). (ii) The rate of H_2O_2 formation was determined using a horseradish peroxidase coupled assay. The reaction was followed by excitation at 325 nm and monitoring the fluorescence emission at 415 nm (slits = 1.5 nm) to quantitate the rate of formation of H_2O_2. The standard assay conditions were the same as the UV A_{240} assay with the addition of 1.0 m*M* *p*-hydroxyphenylacetic acid and 10 U horseradish peroxidase. When buffer *C* was used, 2,2′-azinobis(3-ethylbenzothiazoline-6-sulfonate) (ABTS) was used to reduce H_2O_2 in the presence of horseradish peroxidase and the increased absorbance was followed at 600 nm (ε_{600} = 18 200 M^{-1} cm^{-1}). Independent sets of data were simultaneously fitted to the hyperbolic form of the Michaelis–Menten equation using *Kaleidagraph* (Synergy Software, Reading, Pennsylvania, USA).

2.9. Redox-potential measurements

Potentiometric titrations were performed to determine the midpoint potential of WT and mutant cholesterol oxidases. Methyl viologen (100 μM) was used as the mediator dye to transfer electrons from the electrode to the protein and the redox indicator dye. For WT cholesterol oxidase (20–30 μM), indigo disulfonate, 2-amino-1,4-naphthoquinone and cresyl violet were used as redox indicator dyes. For N485D and N485L mutant cholesterol oxidases (20–30 μM) riboflavin was used. Before each titration, the enzyme solutions (in 50 m*M* sodium phosphate pH 7.0 or 50 m*M* citrate phosphate pH 5.1) underwent 12 cycles of vacuum and argon purging over 2 h to reach an anaerobic state. The electrodes (working, auxiliary and reference electrodes) were then inserted into the spectroelectrochemical cell under positive argon pressure and the titration was initiated by adding electrons from a potentiostat (Model 800B, CH Instruments, Austin, Texas, USA). After each addition of electrons, the system was allowed to equilibrate at 298 K for 30 min and a spectrum was then recorded as well as the potential. The redox-indicator dyes were titrated under the same conditions as the enzyme and their spectra were subtracted to obtain the spectra of enzyme alone. The concentrations of all species of the enzyme were calculated from the spectra and their molar absorptivities and were plotted *versus* the equilibrium potential of the system using

$$E_{cell} = E^{\circ\prime}_{enzyme} + 0.059 \log[ox/red]. \quad (1)$$

The potential of the enzyme, $E^{\circ\prime}_{enzyme}$, equalled the value of the *y* intercept.

3. Results

3.1. Steady-state kinetics and potentiometry at pH 7

The kinetic proficiencies of the N485D, N485L and WT cholesterol oxidases are shown in Table 2. The parameters were measured at steady state following hydrogen-peroxide formation with cholesterol as a substrate. Since cholest-4-en-3-one was the final product, this assay monitored the oxidation of cholesterol and isomerization of the intermediate. The k_{cat} of N485D was diminished ∼650 times compared with that of WT and that of N485L was reduced ∼1100-fold. The apparent K_m values are minimally affected by the N485D and N485L mutations. The intermediate cholest-5-en-3-one was used as a substrate to probe the isomerization step only. The mutations at residue 485 affected the isomerization rate to a lesser extent than substrate oxidation (Table 2). The kinetic isotope effects for WT and the mutants are shown in Table 3. Hydride transfer remains the rate-determining step for the WT enzyme at both pH 5.1 and pH 7.0. For N485L, hydride transfer also remains rate-determining; however, for N485D it is no longer the rate-determining step for catalysis at pH 5.1 (Table 3).

The redox-potential titrations of the WT, N485D and N485L cholesterol oxidases were conducted using an anaerobic spectroelectrochemical cell and the method of Stankovich (1980, 2002). The potential of the enzyme was poised using a redox dye for which the E_m is within 30 mV of

Table 3
Primary isotope effects for WT and mutant cholesterol oxidases as a function of pH.

	Enzyme	^{D}V†	$^{D}V/K$†
pH 5.1	WT	1.9 ± 0.1	1.6 ± 0.1
	N485D	1.2 ± 0.1	1.2 ± 0.1
	N485L	2.4 ± 0.2	2.4 ± 0.2
pH 7.0	WT	2.2 ± 0.1‡	2.2 ± 0.1‡
	N485D	2.5 ± 0.2	2.5 ± 0.2
	N485L	2.2 ± 0.1‡	2.2 ± 0.1‡

† Measured by H_2O_2 formation using 3-[^{2}H]-cholesterol as substrate. ‡ From Yin *et al.*, 2001.

the enzyme. The potentials were measured with an Ag/AgCl electrode and corrected to the standard hydrogen electrode. The concentrations of oxidized, semiquinone and reduced flavin enzyme species were determined spectroscopically at each measured potential. As summarized in Table 4, E_1 corresponds to the one-electron reduction potential for reduction of the cofactor to the semiquinone form and E_2 indicates the potential of the second electron reduction, which converts the semiquinone of the cofactor to its reduced form. The midpoint potential of the WT enzyme is within the range of potentials that are observed for most flavoproteins (0–∼150 mV) at pH 7.0. The E_m of N485D and N485L are reduced by −80 and −85 mV from that of WT, respectively.

3.2. Kinetic and potentiometric measurements at pH 5.1

The kinetic and thermodynamic parameters of the WT and mutant enzymes were measured at pH 5.1 and compared with the parameters obtained at pH 7.0. For the WT enzyme and the N485L mutant the rate of oxidation was unchanged between pH 5.1 and 7.0, whereas for the N485D mutant the low pH resulted in a 20-fold increase in the rate of oxidation compared with that at pH 7.0 (Table 2). The isomerization step in the WT enzyme remained unchanged over the pH range 4.5–10.6 (Kass & Sampson, 1998). In contrast, the isomerization catalyzed by N485D decreased eightfold at pH 5.1 compared with pH 7.0. The midpoint reduction potentials for WT and mutant enzymes were 58–125 mV more positive when the pH was lowered to 5.1 (Table 4). The change in potential observed between pH 5.1 and pH 7.0 was greater for the mutants than for the WT enzyme (Table 4).

3.3. Atomic resolution structure of the N485L mutant

The structure of the N485L mutant was refined to 0.92 Å resolution. The improved resolution over the previously reported 1.5 Å resolution structure (Yin *et al.*, 2001) provided the data necessary to observe the multiple conformations of amino-acid residues in the active site (Fig. 2*a*). This analysis allowed a rigorous comparison with the atomic resolution structure of the WT enzyme (Lario *et al.*, 2003).

Two conformations of Leu485 are visible in the electron density, only one of which was evident in the 1.5 Å resolution structure. The second conformation differs from the original conformation by a 180° rotation about χ_2, thus positioning CG

Table 4
Redox potentials of WT and mutant enzymes as a function of pH.

n.m., not measurable; n.a., not applicable.

	Enzyme	E_1 (mV)	E_2 (mV)	E_m (mV)	$E_m^{mutant} - E_m^{WT}$ (mV)	$E_m^{pH\ 5} - E_m^{pH\ 7}$† (mV)
pH 7.0	WT	−97 ± 8‡	−165 ± 4§	−131	n.a.	n.a.
	N485D	n.m.	n.m.	−211 ± 6¶	−80	n.a.
	N485L	n.m.	n.m.	−216 ± 2¶	−85	n.a.
pH 5.1	WT††	−28 ± 1	−117 ± 3	−73	n.a	58
	N485D	n.m.	n.m.	−82 ± 4‡‡	−9	125
	N485L	n.m.	n.m.	−103 ± 4‡‡	−30	112

† Decrease in E_m from that of WT. ‡ The average and standard deviation of four experiments (the dyes used were I2S and ANQ). § The average and standard deviation of three experiments (the dyes used were ANQ and CV). ¶ The average and standard deviation of two experiments (the dye used was riboflavin). †† The average and standard deviation of two experiments for each potential (the dyes used were E1, I4S; E2, CV). ‡‡ The average and standard deviation of two experiments (the dyes used were riboflavin and CV).

and the terminal methyl groups of the side chain differently (Fig. 3). The side chain is not positioned near the flavin moiety in either of the observed conformations. Thus, the absence of hydrogen-bond donating atoms on the side chain of residue 485 abolishes the ability of the residue to be positioned near to FAD (Figs. 3*a* and 3*b*). In addition, the higher resolution structure of N485L shows Met122 in two conformations (Fig. 2*a*), even though only one conformation (*B*) is visible in the lower resolution structure.

Although the N485L mutation does not completely restrict the movement of Met122, it nevertheless has a pronounced effect on the alternative conformations of Phe359, one of the residues that is located in the putative oxygen tunnel and that is involved in the gating of this channel (Chen *et al.*, 2008; Lario *et al.*, 2003). In the WT structure, conformation *B* of Asn485 (in which the amide is positioned closer to the isoalloxazine moiety of FAD) is correlated with conformation *B* of Phe359 (in which the phenyl ring has rotated almost 90° compared with conformation *A*), opening a narrow hydrophobic channel between the active site and the bulk solvent (Fig. 4*b*). In the N485L mutant structure, the side chain of Phe359 does not adopt a 'channel-open' conformation (Figs. 4*c* and 4*d*). Rather, the phenyl ring rotates closer to the leucine side chain, maximizing van der Waals interactions and in so doing maintains the tunnel in a closed state.

Glu361 is found in only one conformation in the N485L mutant, which corresponds most closely to conformation *A* in the WT structure. However, the side chain refined with only 50% occupancy and there is no additional observed density for the remaining side chain. This suggests that the side chain is either highly mobile or may have undergone loss of the carboxylate moiety owing to radiation damage. In the conformation observed, the side chain lies closer to the active site and contributes to the region of high electron density known as the 'electrostatic patch' that is proposed to play a role in substrate deprotonation (Lario *et al.*, 2003). The side-chain carboxylate O atom OE1 of Glu361, which makes a 3.2 Å hydrogen-bond contact to Asn485 ND1 in conformation *A* in the WT structure, is positioned 3.3 and 3.7 Å away from

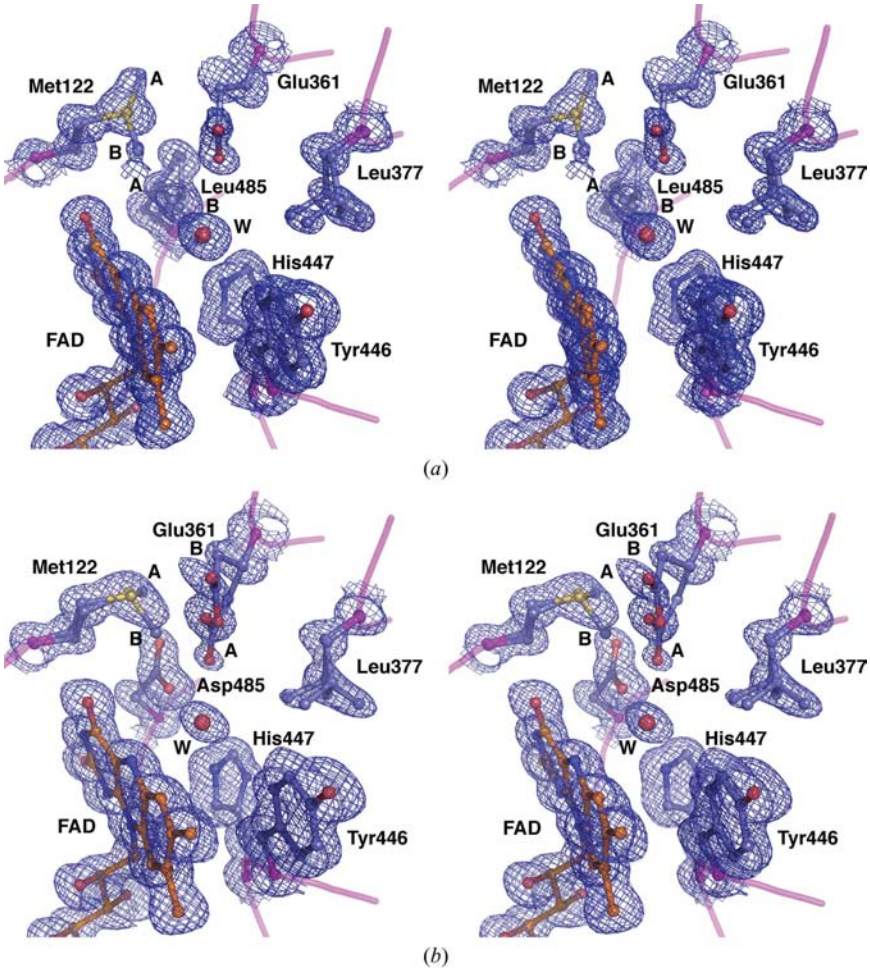

Figure 2
Electron density of cholesterol oxidase active site. $2F_o - F_c$ electron density (blue mesh), contoured at 1.0σ, is shown for (*a*) the N485L mutant and (*b*) the N485D mutant. Active-site residues and the FAD cofactor are shown as ball-and-stick models. Alternate conformations of side chains have been labeled *A* and *B*.

Leu485 CD2 in conformations *A* and *B*, respectively. It is noteworthy that in the N485L mutant structure Glu361 is preferentially oriented towards the active site rather than away from it. This suggests that Glu361 occupies conformation *A* by default and adopts conformation *B* by rearrangement of the active site during WT catalysis.

3.4. Atomic resolution structure of the N485D mutant

The structure of the N485D mutant refined to 1.0 Å resolution reveals extensive disruption of the active site. The side chain of Asp485 is found in a single conformation identical to that of conformation *A* of the asparagine side chain in the WT structure, with the side-chain amide group positioned further away from the isoalloxazine moiety (Figs. 3*a* and 3*c*). A water molecule (Wat1241) found at 42% occupancy in the WT structure and associated with Asn485 is also found hydrogen bonded to Asp485 OD2 in the N485D mutant (Figs. 3*a* and 3*c*). This water molecule is located in a hydrophobic pocket bounded by the side chains of Phe359, Val484 and Val124 and makes a hydrogen-bond interaction with the π electrons of the phenyl ring of Phe359 in conformation *B*.

This water molecule is only present in the 'tunnel-open' arrangement of side chains in the WT structure. In the N485D mutant the tunnel never adopts a tunnel-open structure

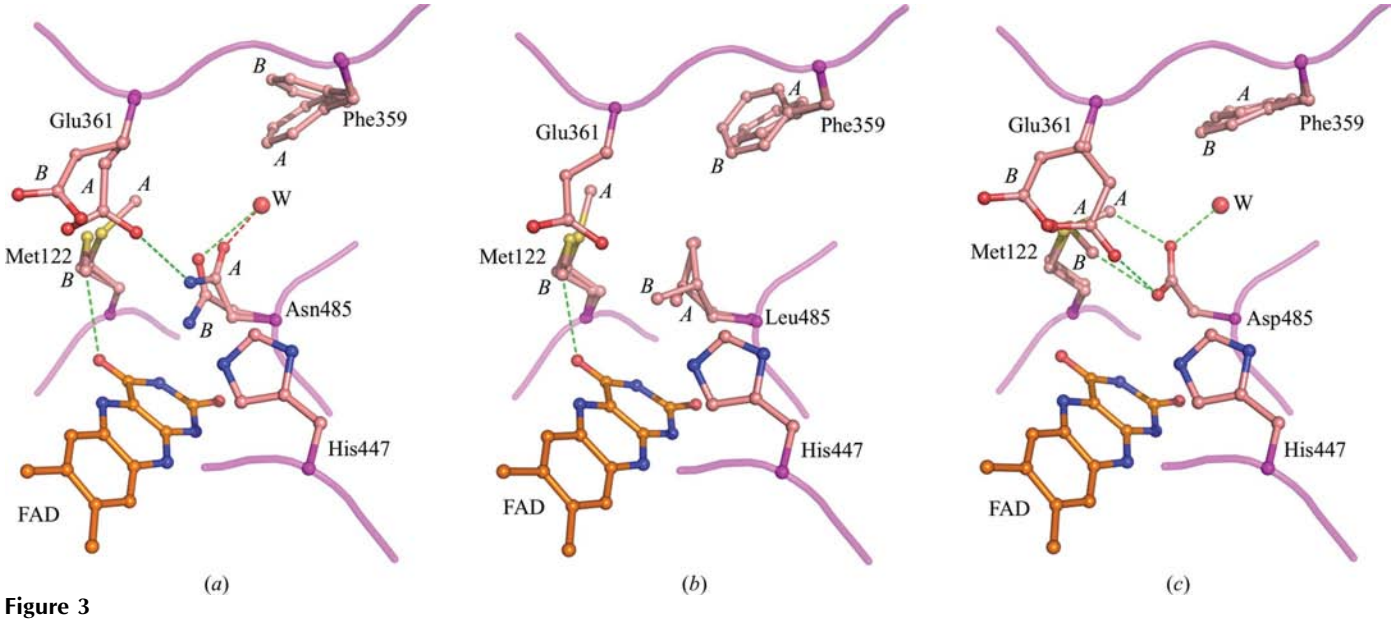

Figure 3
Comparison of cholesterol oxidase active sites. (*a*) WT enzyme, (*b*) N485L mutant, (*c*) N485D mutant. Only the isoalloxazine portion of FAD is shown for clarity. Hydrogen bonds are shown as dashed lines. Water molecules are labeled W. Alternate conformations for side chains are labeled *A* and *B*.

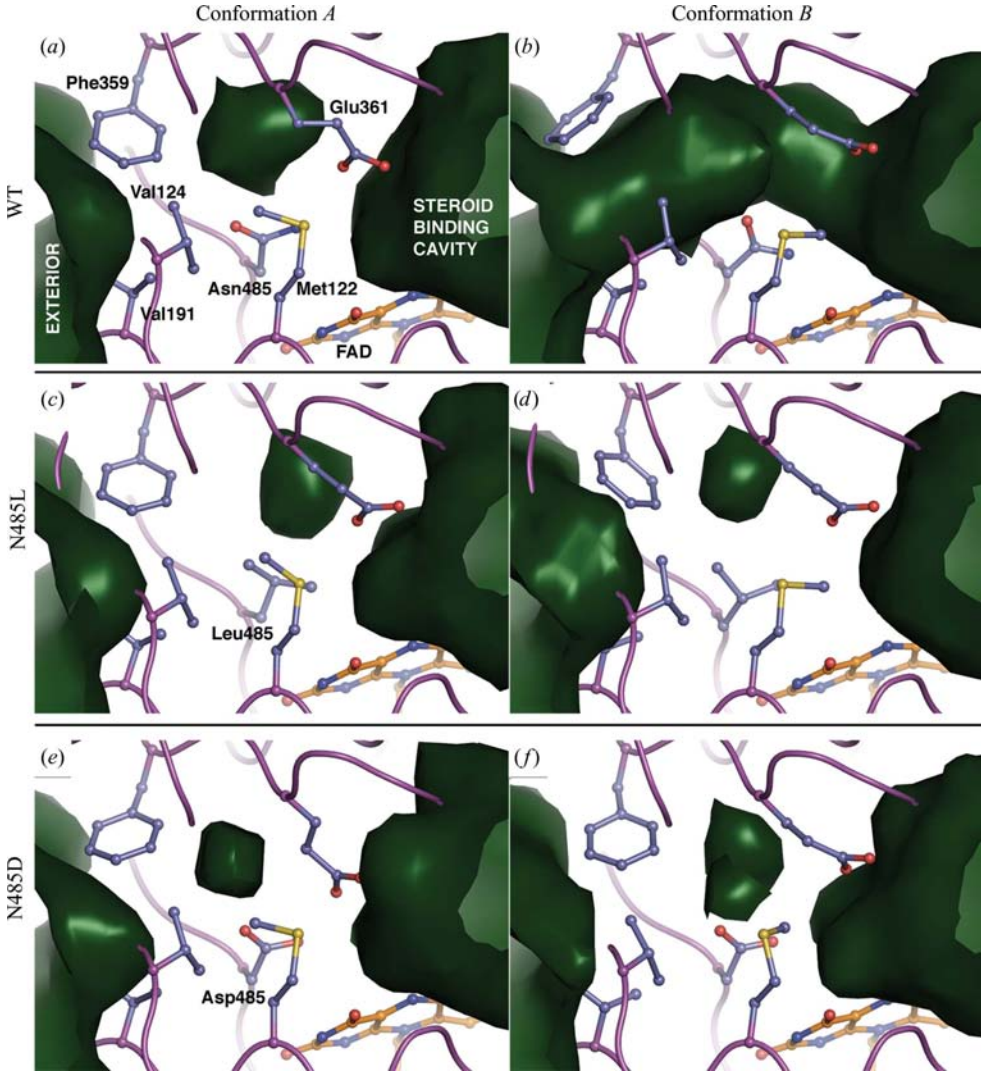

Figure 4
Effect of mutation on the putative oxygen-access channel. (*a*)–(*f*) Space-filling representations of the solvent-accessible surface in the vicinity of the cholesterol oxidase active site. (*a*, *c*, *e*) Active-site residues in conformation *A*, with the channel closed. (*b*, *d*, *f*) Active-site residues in conformation *B*, with the channel open in the WT enzyme. Mobile residues of the (*a*, *b*) WT enzyme, (*c*, *d*) the N485L mutant and (*e*, *f*) the N485D mutant are shown in ball-and-stick representation.

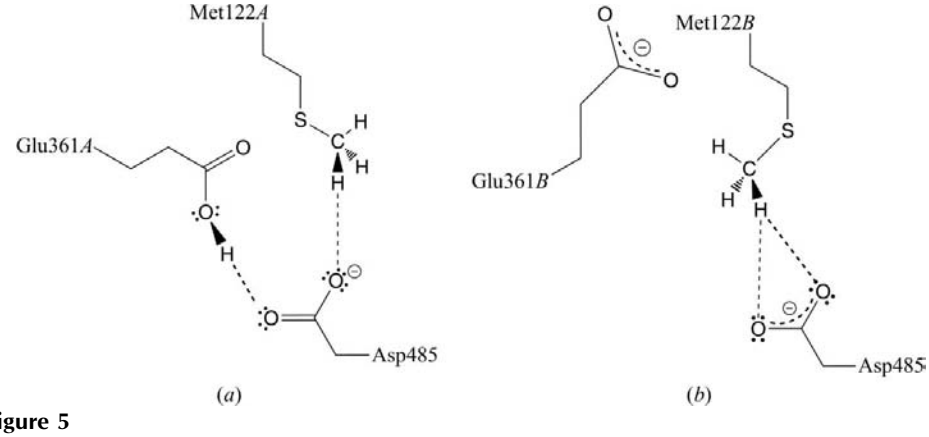

Figure 5
A model of the unusual hydrogen-bonding interactions of Asp485 with Glu361 and Met122. (*a*) Conformation *A*, with Glu361 OE2 protonated and negative charge localized on Asp485 OD2; (*b*) conformation *B*, with Glu361 not protonated and negative charge delocalized on both Glu361 and Asn485. Note that in both cases the methyl of Met122 interacts with negatively charged moieties.

since (i) the aspartate side chain remains more similar to conformation *A* in the WT structure and the carboxylate never moves closer to the pyrimidine-ring system of FAD and (ii) the side chain of Phe359 does not move to the same extent as in the WT structure.

Met122 is found in two conformations, both of which deviate somewhat from their observed positions in the WT structure (Figs. 3*a* and 3*c*). The CE methyl that points away from FAD in conformation *A* and points towards FAD in conformation *B* is now shifted in both conformations towards the carboxylate of Asp485. In conformation *A* the distance between Met122 CE and Asp485 OD2 is 2.46 Å (Fig. 5*a*); in conformation *B* Met122 CE is 2.61 Å from Asp485 OD1 and 2.86 Å from Asp485 OD2 (Fig. 5*b*). Thus, the terminal methyl group on the methionine side chain is involved in unusually short CH···O hydrogen-bond interactions with the aspartate carboxylate moiety.

In addition to the unusual CH···O contact between Asp485 and Met122, a short hydrogen bond is observed between Asp485 and conformation *A* of Glu361, which is shifted even closer to the 485 side chain relative to what is observed in the WT structure (Figs. 3*a* and 3*c*). The close contact between the aspartate carboxylate group and the methyl group of Met122 in both conformations *A* and *B* strongly suggests that Asp485 is anionic in the structure. Furthermore, it suggests that at pH 5.2, the pH at which the crystals were grown, Glu361 is protonated in conformation *A*. It is possible that the second conformation of Glu361 may be unprotonated. However, the mobility and hence partial occupancy of this residue does not allow us to visualize the H atom in the case of a protonated carbox-

ylate group even at the better than 1 Å resolution of the data set. A data set for the mutant collected from crystals at pH 7.0 revealed no differences in side-chain conformations compared with the mutant structure from crystals grown at pH 5.2 (unpublished data), suggesting that the difference in pH does not affect discrete residues in the active site to the extent that the changes are visible in an atomic resolution electron-density map.

4. Discussion

The role of Asn485 in the redox activity and catalysis of oxidation in the flavoenzyme cholesterol oxidase was studied. Mutations of this side chain were made to alter the electrostatic character at the active site and the kinetic and redox activities of the mutants were determined and compared with those of the WT enzyme at two different pH values. In all cases the mutations had a minimal affect on the apparent Michaelis constant for the steroid substrate; only k_{cat} was affected by the mutations and the pH.

In the WT enzyme, similar kinetic constants were observed at pH 5.1 and 7.0. However, an increase in the midpoint reduction potential at pH 5.1 relative to that at pH 7.0 indicates that the flavin cofactor is more readily reduced at lower pH. This suggests that the electrostatic environment around the active site plays an important role in both catalysis and redox potentiation of the cofactor. Comparisons of the WT structures determined at ~0.95 Å resolution from crystals of the enzyme grown at pH 5.2 and at pH 7.0 failed to show any obvious structural changes within this pH range (Lyubimov *et al.*, 2006). Atomic resolution structures of the N485D mutant at pH 5.2 and pH 7.0 also did not indicate significant changes (data not shown). Changes in the redox potential induced by pH are likely to arise from effects on the electrostatic environment around the cofactor. The refinement methods most commonly used in macromolecular crystallography utilize a spherical free-atom model which does not take into account any deformation of the valence electron density resulting from chemical bonding or intermolecular interactions. Thus, imposing a spherical-atom model may mask changes in the electrostatics of the active site which affect the electron distribution. Approaches are being developed to incorporate a multipole model of the atoms which takes into account the charge density and thus allows a more accurate representation of the electrostatic properties within a molecule (Jelsch *et al.*, 2005; Lecomte *et al.*, 2005). However, such approaches typically require crystallographic diffraction data significantly higher than 0.9 Å resolution. Thus, a more accurate structural study of the electronic effects of pH and mutation in the cholesterol oxidase active site will require diffraction data at resolutions that exceed 0.9 Å.

In order to compare the effect of electrostatics on redox activity, the asparagine side chain at position 485 in the enzyme was mutated to both an aspartate and a leucine. Analysis of the kinetic constants of these mutations revealed a decrease in oxidation activity at pH 7.0 for both mutants and a smaller decrease in isomerization relative to the WT enzyme (Table 2). At pH 5.1, partial recovery in oxidation was evident for N485D but not for N485L and a decrease in isomerization was observed for N485D. Previous structural and kinetic studies concluded that Asn485 gates the oxygen channel by stabilization of the reduced cofactor through an NH$\cdots\pi$ interaction between the asparagine NH and the pyrimidine ring of the cofactor (Lario *et al.*, 2003; Yin *et al.*, 2001). Thus, Asn485 is involved in hydrogen-bond donating interactions that are important both kinetically and thermodynamically. In the N485D structure, determined with crystals grown at pH 5.2, the carboxylate group of aspartate is involved in hydrogen-bond interactions with one conformation of Glu361 and both conformations of Met122. The glutamate side chain involved in this contact adopts a conformation different from either *A* or *B* in the WT structure. Glu361 plays a role in oxidation through the formation of a proton relay needed for deprotonation of the alcohol during oxidation (Lario *et al.*, 2003). In the isomerization step, Glu361 transfers an H atom from C4 to C6 of the steroid substrate (Kass & Sampson, 1995; Sampson & Kass, 1997). Thus, the position and protonation state of Glu361 are critical for both oxidation and isomerization activity.

The different position of Glu361 in the N485D mutant arising from the observed hydrogen-bond interaction with Asp485 affects both steps of catalysis: oxidation and isomerization. The close proximity of the aspartate and glutamate side chains strongly suggests the presence of an H atom on one of these side chains or shared between them. Unfortunately, the multiple conformations of Glu361 adversely affect our ability to visualize this H atom even at the high resolution of the structure. However, it can be inferred that the proton lies closer to Glu361 since (i) Asp485 is also involved in a very short hydrogen bond to the methyl H atoms of Met122 and such an interaction would most likely require a negatively charged carboxylate group (Derewenda *et al.*, 1995; Fig. 5) and (ii) the isomerization activity at pH 5.1 decreases, most likely owing to the partial protonation of Glu361, which would interfere with the abstraction of the substrate C4 proton required for isomerization. As a result, mutation of Asn485 to an ionized aspartate adversely affects the kinetics of both oxidation and isomerization through mispositioning the side chain of Glu361 and altering its protonation state.

As for the N485D mutant, the rate of oxidation by the N485L mutant decreases at both pH 5.1 and 7.0 and its isomerization activity decreases at pH 7.0 (Table 2) compared with the WT enzyme. While the N485D mutant could successfully recover some activity at lower pH, the N485L mutant failed to show any improvement in oxidation chemistry. The structure of the N485L mutant reveals only one position for Glu361. In the WT structure a hydrogen-bond interaction between conformation *A* of Asn485 and Glu361 holds the glutamate in a position that contributes to the formation of the proton relay. In the leucine mutant, the poor hydrogen-bonding capability of the leucine side chain weakens this interaction; although an aliphatic hydrogen-bond interaction is seen between the leucine methyl group and the glutamate carboxylate, it is not as close as that between

Asn485 and Glu361 in the WT structure. Thus, the electrostatic environment required to form the relay needed for oxidation is not present.

For both mutants, the side chain of residue 485 adopts positions away from the pyrimidine ring (Fig. 3), thus no NH$\cdots\pi$ interaction with the cofactor is observed. Furthermore, for both mutations, the side chain affects the position of Glu361 and thus the proposed proton relay needed for deprotonation of the substrate hydroxyl H atom. In the N485L mutant the hydrophobic nature of the side chain reorients the glutamate side chain of Glu361 away from conformation *A*, which in the WT structure enables substrate oxidation. In the N485D mutant the short hydrogen-bond interactions between Asp485 and Glu361 result in positioning of the glutamate side chain so that it lies closer to the aspartate group, hence misorienting the glutamate for efficient oxidation. Thus, through different orientation effects on Glu361, each of the mutations alters the position of the glutamate in such a way as to adversely affect efficient substrate oxidation. In the case of N485D this loss of activity is partially recoverable at lower pH, where the aspartate side chain becomes partially protonated and thus more like an asparagine side chain in terms of its hydrogen-bonding capabilities. As seen in the structure (determined with crystals grown at pH 5.2), the side chain of Glu361 is able to adopt conformation *B* but the hydrogen-bond interaction between Asp485 and both conformations of Met122 eliminates the ability of the protonated aspartate to move to conformation *B* nearer to the pyrimidine moiety (Fig. 5). For the WT enzyme the structure reveals Asn485 in both conformation *A* and *B*; no strong hydrogen-bond interactions are seen between Asn485 and either conformation of Met122, thus the electrostatic interaction between these two residues is not so strong as to hold the asparagine side chain in conformation *A*. On the other hand, the strong electrostatic interaction between Asp485 and Met122 stabilizes the aspartate in a single conformation closer to that of conformation *A* in the WT structure.

5. Conclusions

Structural and enzymological characterizations of two cholesterol oxidase mutants illustrate the importance of asparagine at position 485 to the redox potential and catalytic efficiency of the enzyme. Atomic resolution structures of N485L and N485D mutants show that the mutations affect the positioning of Glu361 and hence the proton relay needed for substrate oxidation and the base needed for isomerization. In addition, the interactions with the mutant side chains abolished the NH$\cdots\pi$ interaction with FAD and correlate well with the observed drop in the redox potential of the enzyme. Both the redox midpoint potential and substrate turnover are dependent on pH. Thus, the pH affects the electrostatic nature of the active site and hence the ability of the structure to stabilize the reduced cofactor. These observations demonstrate that the Asn485 residue plays a central role in the reaction catalyzed by cholesterol oxidase by affecting the electrostatic and hydrogen-bonding network necessary for multiple chemical and conformational steps of the catalytic mechanism.

We acknowledge the gracious help of Professor Marian Stankovich in determining reduction potentials.

References

Berman, H. M., Westbrook, J., Feng, Z., Gilliland, G., Bhat, T. N., Weissig, H., Shindyalov, I. N. & Bourne, P. E. (2000). *Nucleic Acids Res.* **28**, 235–242.

Chen, L., Lyubimov, A., Brammer, L., Vrielink, A. & Sampson, N. S. (2008). *Biochemistry*, **47**, 5368–5377.

Christopher, J. A. (1998). *The SPOCK Program Manual.* http://quorum.tamu.edu/Manual/Manual/Manual.html.

Collaborative Computational Project, Number 4 (1994). *Acta Cryst.* D**50**, 760–763.

DeLano, W. L. (2002). *The PyMOL Molecular Graphics System.* DeLano Scientific, San Carlos, California, USA.

Derewenda, Z. S., Lee, L. & Derewenda, U. (1995). *J. Mol. Biol.* **252**, 248–262.

Emsley, P. & Cowtan, K. (2004). *Acta Cryst.* D**60**, 2126–2132.

Jelsch, C., Guillot, B., Lagoutte, A. & Lecomte, C. (2005). *J. Appl. Cryst.* **38**, 38–54.

Kass, I. J. & Sampson, N. S. (1995). *Biochem. Biophys. Res. Commun.* **206**, 688–693.

Kass, I. J. & Sampson, N. S. (1998). *Biochemistry*, **37**, 17990–18000.

Kraulis, P. J. (1991). *J. Appl. Cryst.* **24**, 946–950.

Lario, P. I., Sampson, N. & Vrielink, A. (2003). *J. Mol. Biol.* **326**, 1635–1650.

Laskowski, R. A., MacArthur, M. W., Moss, D. S. & Thornton, J. M. (1993). *J. Appl. Cryst.* **26**, 283–291.

Lecomte, C., Guillot, B., Jelsch, C. & Podjarny, A. (2005). *Int. J. Quant. Chem.* **101**, 624–634.

Linder, R. (1997). *Emerg. Infect. Dis.* **3**, 145–153.

Lyubimov, A. Y., Lario, P. I., Moustafa, I. & Vrielink, A. (2006). *Nature Chem. Biol.* **2**, 259–264.

Merritt, E. A. & Bacon, D. J. (1997). *Methods Enzymol.* **277**, 505–525.

Murshudov, G. N., Vagin, A. A. & Dodson, E. J. (1997). *Acta Cryst.* D**53**, 240–255.

Navas, J., Gonzalez-Zorn, B., Ladron, N., Garrido, P. & Vazquez-Boland, J. A. (2001). *J. Bacteriol.* **183**, 4796–4805.

Otwinowski, Z. & Minor, W. (1997). *Methods Enzymol.* **276**, 307–326.

Sampson, N. S. & Kass, I. J. (1997). *J. Am. Chem. Soc.* **119**, 855–862.

Sheldrick, G. M. (2008). *Acta Cryst.* A**64**, 112–122.

Stankovich, M. T. (1980). *Anal. Biochem.* **109**, 295–308.

Stankovich, M. (2002). *Encyclopedia of Electrochemistry*, Vol. 9, *Bioelectrochemistry*, edited by G. S. Wilson, pp. 487–509. Weinheim: Wiley-VCH.

Tomioka, H., Kagawa, M. & Nakamura, S. (1976). *J. Biochem.* **79**, 903–915.

Uwajima, T., Yagi, H. & Terada, O. (1974). *Agric. Biol. Chem.* **38**, 1149–1156.

Vaguine, A. A., Richelle, J. & Wodak, S. J. (1999). *Acta Cryst.* D**55**, 191–205.

Vrielink, A., Lloyd, L. F. & Blow, D. M. (1991). *J. Mol. Biol.* **219**, 533–554.

Yin, Y., Sampson, N. S., Vrielink, A. & Lario, P. I. (2001). *Biochemistry*, **40**, 13779–13787.

Yue, Q. K., Kass, I. J., Sampson, N. S. & Vrielink, A. (1999). *Biochemistry*, **38**, 4277–4286.